Progress Report F6

25-11-2022

Mitch Robson (mitch.robson@ambature.com)
Priyanka Brojabasi (priyanka.brojabasi@ambature.com)
Archana Tiwari (archana.tiwari@ambature.com)

Contents

1 Summary

We report on the recent progress in the fabrication and measurement of Josephson junctions in F6. Until F5, we were using the PBCO as an insulating layer between the top and bottom YBCO contacts, which reduces the device's robustness upon application of a higher current bias. In F5, the magnetic field dependency of the Josephson junction to obtain the Fraunhofer pattern was also unexplored.

The major fabrication leap in F6 was to include a SiO_2 insulating layer as a barrier between the top and bottom YBCO contacts. We explored various methods of creating a via through SiO_2 layer without affecting the YBCO, including (1) lift-off, and (2) Reactive Ion Etching (RIE) of SiO_2. We concluded that RIE etching with an etch stop layer of Au is the most robust method. On the measurement side, we used the Physical Property Measurement System (PPMS) from Quantum Design to characterize Josephson junctions. We measured the conventional IV characteristics, and Fraunhofer plots to show the magnetic field dependence of the critical current.

To increase the efficiency, we included checkpoints at various stages of fabrication, including XRD and room temperature probing, to confirm the quality of the device.

2 Introduction

The main objectives for F6 can be divided into two sections, 2.1 Fabrication, and 2.2 Measurement.

2.1 Fabrication

- Adding insulating SiO_2 layer
- Reproducible JJs
- SQUID design

Through the various iterations of F6, we made progress on different fronts of developing a device. This includes changes in the design, fabrication processes, and measurement techniques. In the design changes, we modified the Josephson junction design to include complete junction characterization, four-probe measurements, and testing for the maximum device density. We changed the SQUID design to reduce the charging during the FIB process, and to incorporate different sculpting ideas for the SQUID. In the fabrication changes, we switched the deposition processes from electron beam deposition to sputtering to increase the film quality. An etch stop layer of Au was introduced, to protect the YBCO layer from etching during the SiO_2 via formation, and to enhance the contact quality. Figure 1 compares the F5 and F6 designs. Additionally, we reduced the junction area to 2 x 2 μm^2, the limit of the current photolithography in the Waterloo clean room. In the measurement, we started using PPMS, owing to its fast cooling down, temperature stability, and ease of operation. We also explored the magnetic field dependence of the critical current to obtain the Fraunhofer plot between the critical current and magnetic field.

F6 includes 12nm of PBCO sandwiched between two 100 nm thick layers of YBCO, while F5 had 8nm of PBCO sandwiched between two 64nm layers of YBCO. The thickness difference between the YBCO and PBCO between F5 and F6, impacts the room temperature resistance, transition temperature, and critical current passing through the junction. A SQUID consists of a superconducting loop interrupted by two Josephson junctions. F6 SQUID is carved based on the reference [3]. The sensitivity of a SQUID sensor towards magnetic field depends on the SQUID loop area.

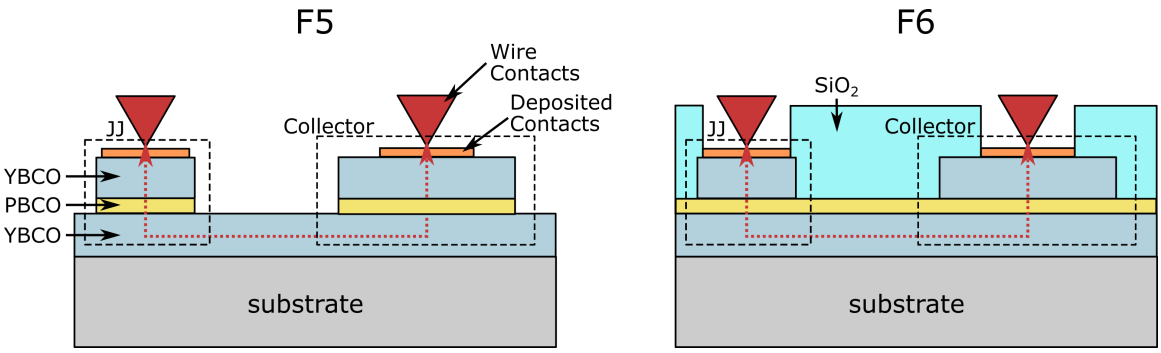

Figure 1: A comparison between design of F5 and F6. F6 includes an insulating layer of SiO_2 to separate contacts attached to the top and bottom YBCO layers.

Figure 2 shows an SEM micrograph of the F6 Josephson junction involving collector and 4-probe transport measurement contacts and F6 SQUID. A 250 nm of SiO_2 is sputtered based on the dielectric constant of SiO_2 and the thickness of each YBCO layer to separate the bottom and top contacts.

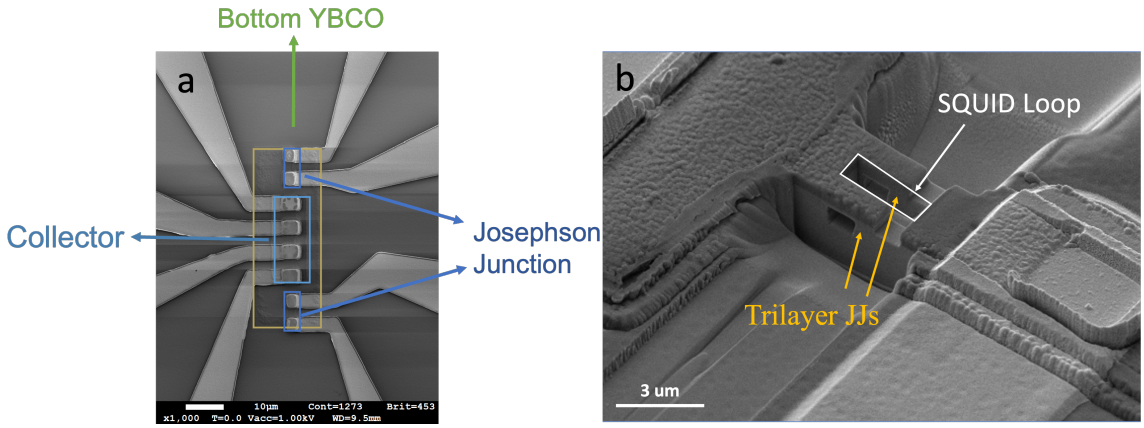

Figure 2: A SEM image of an F6 Josephson junction and SQUID. (a) Josephson Junction device shows the junction with an area of $4\mu m^2$, a collector, and 4-probe contacts. (b) SEM image shows the SQUID loop and trilayer JJs.

To increase the efficiency and reproducibility, we included additional XRD characterization before starting the device fabrication to ensure the quality of the YBCO film; and room temperature probe to ensure the contact resistance before loading the sample into the cryostat. The quality of a-axis YBCO was confirmed through the XRD measurement before starting the fabrication Figure 3 shows the XRD data and corresponding peak (200) of a-axis YBCO at 47.5 deg for F6, this matches with the 2θ values of the XRD data from the original Cornell sample, as shown Fig 2 of reference [5].

2.2 Measurement

- Exploring alternative measurements systems: PPMS
- Magnetic field dependency of the critical current: Fraunhofer Pattern

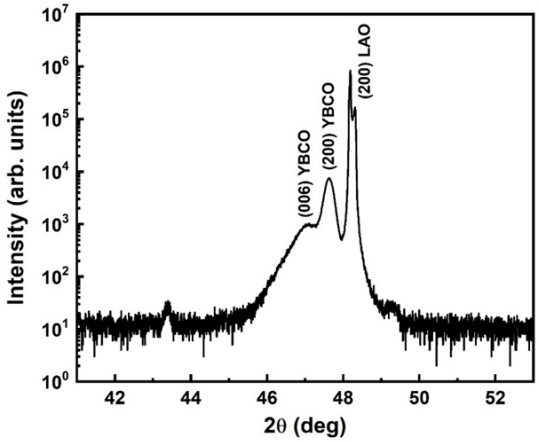

Figure 3: XRD data of the YBCO before starting the fabrication shows peak (200) for a-axis YBCO at 47.5 deg.

2.2.1 Physical Property Measurement System (PPMS)

PPMS DynaCool is a cryogen-free, variable temperature cryostat with temperature ranging from 1.8 to 400K, and an available magnetic field up to 9T. It is designed to perform various automated measurements and has a cool down time of 40 minutes, which helps carrying out the measurements in a time-efficient manner. It uses a two-stage Pulse Tube cooler to cool the superconducting magnet and the temperature control system, providing a low-vibration environment for sample measurements.

The current PPMS system has only AC electric transport measuring module but can be extended to add a DC module, if required. The Electrical Transport Option (ETO) uses a digital lock-in technique to measure in a 4-probe configuration. It also provides an in-built IV curve profiling and differential resistance measurement, these are the specific measurements needed to characterize Josephson junctions. Figure 4a shows the puck used in the current PPMS measurements; it has three 4-probe channels and one optional channel.

2.2.2 Magnetic field dependency of the critical current: Fraunhofer Pattern

In a static condition, the current and superconducting phase across a Josephson junction follows the relation in equation 1. The phase difference (δ) across the junction remains constant.

$$\begin{aligned} I &= I_J(\delta) \\ \frac{d\delta}{dt} &= \frac{2e}{\hbar}V \end{aligned} \tag{1}$$

In the presence of a magnetic field, phase difference along the barrier changes according to the equation 2:

$$\frac{\partial\delta}{\partial x} = \frac{2\pi}{\phi_0}\phi = \frac{2e}{\hbar}B \times \textit{(Effective barrier thickness)} \tag{2}$$

A change in the critical current is observed such that critical current is maximum at zero magnetic field and reduces upon increase the magnetic field in either positive or negative directions. Critical current varies with the following relation upon changing the flux(ϕ), where the flux is defined as the B×(Area of the junction). Figure 4b shows the Fraunhofer pattern obtained from YBCO/PBCO/YBCO trilayer junction [2].

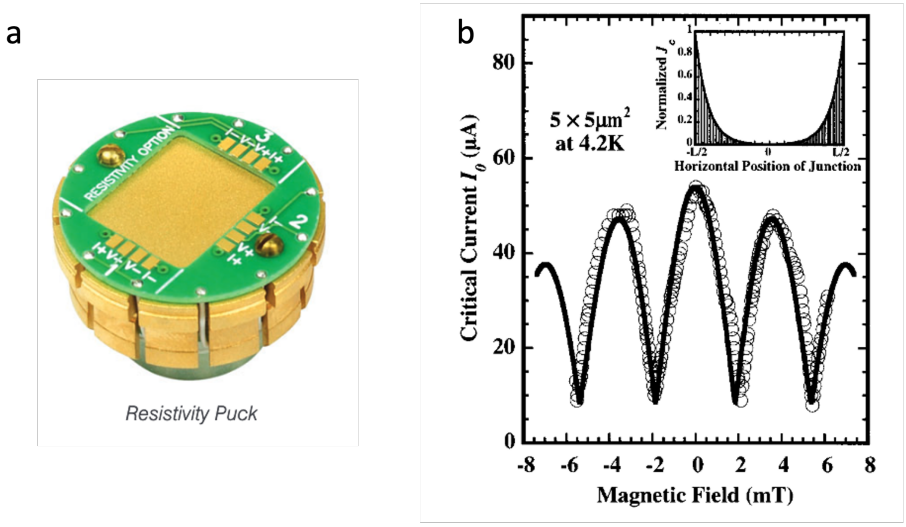

Figure 4: (a) A typical puck to load devices for electrical transport measurement in the PPMS. (b) Fraunhofer pattern shown for YBCO/PBCO/YBCO trilayer junction in reference [2]

$$I_c(\phi) = I_c(0)\frac{\sin(\frac{\pi\phi}{\phi_0})}{\frac{\pi\phi}{\phi_0}} \tag{3}$$

2.2.3 Superconducting Quantum Interference Device (SQUID)

A SQUID is formed when a superconducting loop contains one or more Josephson junctions. It can be used as a highly sensitive detector for magnetic flux or any quantity that can be converted into a magnetic flux. A SQUID operates on two basic principles: 1. Flux quantization, and 2. Superconducting tunneling. Based on the functionality, there are two types of SQUIDs: 1. RF SQUID, and 2. DC SQUID. Table 1 shows a comparison between the RF and DC SQUIDs. There are four parameters deciding the functionality of a SQUID: 1. Inductance (L) of the SQUID loop, 2. Junction critical current (I_c), 3. Shunt resistance (R) per junction, and 4. Parasitic junction capacitance (C). To achieve a particular functionality from a SQUID circuit, these parameters are optimized through simulations before fabricating a device.

	RF SQUID	DC SQUID
1	Superconducting loop has one JJ	Superconducting loop has 2 JJs connected in parallel
2	Driven by high frequency signals applied to a tank circuit magnetically coupled to SQUID	Driven by a direct current
3	Easy to fabricate but has a high noise level	Complex fabrication but lower noise
4	Obsolete for current applications	Useful in recent applications

Table 1: Difference between RF and DC SQUID

3 Results and Analysis

To determine the quality of the Josephson junction and the corresponding characteristic value for critical current and transition temperature the following measurements were performed.

- Superconducting transition: R vs T
- Characteristic IV curve: Signature curve to verify a Josephson junction
- Magnetic field dependency: Fraunhofer pattern

3.1 Superconducting transition: R vs T

Device fabrication in F6 has additional heating and cleaning steps causing a broadening in the transition temperature. Figure 5a shows a superconducting transition in F6, the transition starts at 75K, but due to the broadening of the transition, zero resistance temperature is reached around 50K. The rise in resistance at a lower temperature can be attributed to the increased contact resistance at lower temperatures.

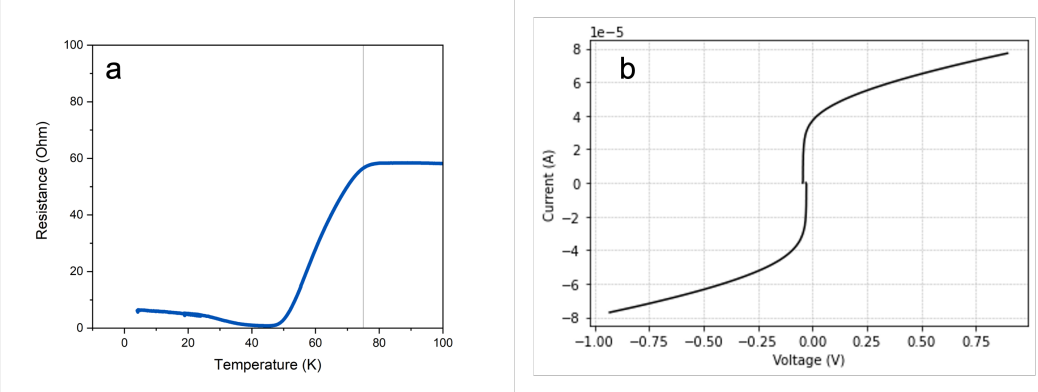

Figure 5: (a) Superconducting transition in the top layer of YBCO of F6. (b) IV characteristics of two Josephson junctions formed by 100nm/12nm/100nm of YBCO/PBCO/YBCO.

3.2 Characteristic IV curve: Signature curve to verify a Josephson junction

A characteristic IV curve indicates a critical current for which zero voltage is measured across the Josephson junction. Figure 5b shows the characteristic IV curve for a Josephson junction in F6.

The critical current calculated from the intercept of linear fitting of the resistive region of the IV curve at 2K is 4.7x10^{-5}A, with a critical current density of 1175A/cm^2. For F5, which has a barrier layer (PBCO) thickness of 8 nm, the critical current density was 150A/cm^2. The critical current density for **F6 is 7.8 times larger than the F5, even with a large barrier thickness**. It can be argued that the junction area for F6 is three times smaller than F5, which is attributed to the increased current density. However, a thick barrier would exponentially decrease the critical current passing through a junction. Therefore, we can confidently say that F6 is an improvement over F5 Josephson junction, owing to its large critical current density and I_cR_N factor. I_cR_N values define the junction frequency and drive various JJ-based applications (RSFQ, JPU clock cycles, etc.). Higher I_cR_N relates to higher frequency JJs, as $f_c = \frac{2e}{h} I_c R_N$. I_cR_N factor controls the noise level in a SQUID, ultimately determining the sensitivity of SQUID-based sensors. A higher I_cR_N is indicative of lower background noise and higher sensitivity. I_cR_N factor in **F6 is ten times larger than the F5**, indicating that

these improvements can be directly beneficial for sensor devices. Table 2 shows a comparison between different fabrication runs F3, F5, and F6 and compares them with an external c-axis reference.

Source	Critical Current Density (A/cm^2)	$I_cR_N(\mu V)$	JJ Area (μV^2)	Barrier	Thickness (nm)	YBCO Type
F6 JJ2	1175	1.35 x 10^6	2 x 2	PBCO	12	a-axis
F5 JJ1	150	3.1 x 10^5	2 x 6	PBCO	8	a-axis
F3	1.8	7.3 x 10^5	250 x 250	PBCO	8	a-axis
[4]	110	160	5 x 5	PBCO	10	c-axis

Table 2: Summary of our JJ characteristics as compared to the literature

3.3 Magnetic Field Dependency: Fraunhofer Pattern

Critical current modulates upon applying a magnetic field to favor thermodynamically stable quantum states. This gives a quantum interference pattern similar to optical single or double slit experiments called Fraunhofer pattern. The periodicity at which critical current becomes 0 indicates the magnetic field corresponding to the flux quantum, $\phi_0 = 2.067$ x10^{-15} Wb.

In F6, we obtained the Fraunhofer pattern by changing the magnetic field in steps and measuring the IV curve at each stage. We then calculated the critical current value for each magnetic field separately. The magnetic field range we explored is from -1.5 to 1.5 mT. In Figure 6, we have plotted the normalized critical current for the normalized flux. The maximum value is observed at zero magnetic field, and the periodicity in the pattern corresponds to the flux quantum ϕ_0.

A constant modulation period of the interference pattern confirms the experimental junction size is consistent with the estimated value. An ideal Fraunhofer pattern has a larger central lobe corresponding to zero magnetic field and smaller lobes for non-zero magnetic field values. In F6, the sidelobes are as large as the central lobe, possibly due to the nonuniform critical current density (J_c) of the junction [2].

3.4 SQUID Measurement

We performed the SQUID measurement in a PPMS. IV characteristics were measured for magnetic field values ranging from -10 mT to +10 mT with a step size of 1 μT. The measured SQUID has a loop area of 1 x 3 μm^2. Figure 7 shows the variation in the voltage obtained at a constant current bias of ± 3 μA with respect to the normalized magnetic flux. According to flux quantization, at a constant current bias, voltage across the junction should change with a periodicity of flux quantum ϕ_0. As seen in Figure 7, the average periodicity obtained in our data is 0.64 ϕ_0.

4 Conclusion and Future Plan

In F6, we have demonstrated a significant improvement over previous JJ iterations, F5 and F3. The Josephson junction in F6 shows a large critical current density and Fraunhofer measurement indicating a robust design and an improved junction quality. Additionally, we measured a FIB sculpted SQUID from F6, and the voltage across the JJ shows periodic oscillations with the magnetic flux.

Since the fabrication of JJs has been considerably improved, our focus in the next iteration will shift on carrying out new measurements to get a complete JJ characterization. The future plans for both measurement and fabrication related goals are listed below.

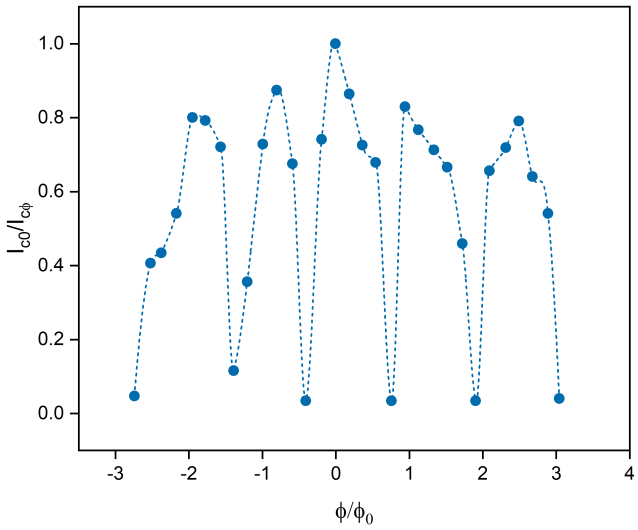

Figure 6: Magnetic field dependency: Normalized critical current with respect to the normalized magnetic flux.

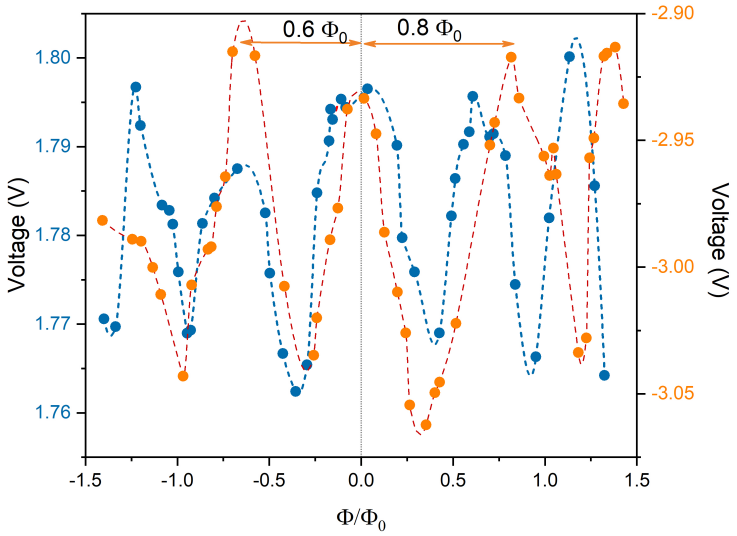

Figure 7: Variation in the voltage with normalized flux at a constant current bias of +3μA (blue) and -3μA (orange).

4.1 Measurement

- Improving Fraunhofer plot by carrying out dense magentic field measurements
- Temperature dependence of the critical current
- Differential resistance measurement

- Shapiro Step measurement
- Critical current dependency on a Junction area
- Critical current dependency on the barrier thickness

4.2 Fabrication

- Removing collector by trying various ion-milling and wet etching methods
- Enhancing device efficiency
- Exploring Josephson junction based superconducting circuits

References

[1] Dietmar Drung. Introduction to Nb-based squid sensors. *IEEE/CSC and ESAS SUPERCONDUCTIVITY NEWS FORUM (global edition)*, April 2016.

[2] E. Fujimoto, H. Sato, T. Yamada, and H. Akoh. All $YBa_2Cu_3O_{7-\delta}$ trilayer junctions with $YBa_2Cu_3O_{7-\delta}$ wiring layers. *Applied Physics Letters*, 80(21):3985–3987, 2002.

[3] Carmine Granata, Antonio Vettoliere, Roberto Russo, Matteo Fretto, Natascia De Leo, and Vincenzo Lacquaniti. Three-dimensional spin nanosensor based on reliable tunnel josephson nano-junctions for nanomagnetism investigations. *Applied Physics Letters*, 103(10):102602, 2013.

[4] Ken'ichi Kuroda, Yukihiko Wada, Tetsuya Takami, and Tatsuo Ozeki. Fabrication of full high-tc superconducting $YBa_2Cu_3O_{7-x}$ trilayer junctions using a polishing technique. *Japanese Journal of Applied Physics*, 42(8B):L1006, aug 2003.

[5] Y. Eren Suyolcu, Jiaxin Sun, Berit H. Goodge, Jisung Park, Jürgen Schubert, Lena F. Kourkoutis, and Darrell G. Schlom. a-axis $YBa_2Cu_3O_{7-x}/PrBa_2Cu_3O_{7-x}/YBa_2Cu_3O_{7-x}$ trilayers with subnanometer rms roughness. *APL Materials*, 9(2):021117, 2021.